J. Astron. Space Sci. 14(2), 355–366 (1997)

GROUND TRACK ACQUISITION AND MAINTENANCE MANEUVER MODELING FOR LOW-EARTH ORBIT SATELLITE

Byoung-Sun Lee and Jong Won Eun
TT&C Section, Electronics and Telecommunications Research Institute
Yusong P.O.Box 106, Taejon 305-600, Korea
e-mail: lbs@mail.etri.re.kr

Charles E. Webb
KDK Industries
10736 Chestnut Ridge Road, Austin, Texas 78726, U.S.A.

(Received October 31, 1997; Accepted November 20, 1997)

ABSTRACT

This paper presents a comprehensive analytical approach for determining key maneuver parameters associated with the acquisition and maintenance of the ground track for a low-earth orbit. A linearized model relating changes in the drift rate of the ground track directly to changes in the orbital semi-major axis is developed. The effect of terrestrial atmospheric drag on the semi-major axis is also explored, being quantified through an analytical expression for the decay rate as a function of density. The non-singular Lagrange planetary equations, further simplified for nearly circular orbits, provide the desired relationships between the corrective in-plane impulsive velocity increments and the corresponding effects on the orbit elements. The resulting solution strategy offers excellent insight into the dynamics affecting the timing, magnitude, and frequency of these maneuvers. Simulations are executed for the ground track acquisition and maintenance maneuver as a pre-flight planning and analysis.

1. INTRODUCTION

Increasingly, low-earth orbiting satellites have become the preferred platforms for a variety of scientific investigations and telecommunications services. Limited by the Van Allen radiation belts to altitudes less than 1000 km, these orbits share a common dynamic environment (Wertz 1991). The primary factors influencing the evolution of such orbits consist of the geopotential, terrestrial atmospheric drag, and luni-solar gravitation. The relative size of these effects depends on the altitude of the satellite, with the first two perturbations dominating in regions nearer the Earth and the last becoming significant toward the upper altitude bound.

To meet the technical objectives of a particular mission, the orbit must typically be constrained within some tolerance dictated by instrument or operational requirements. Thus, in the presence of

the perturbing accelerations, periodic propulsive maneuvers are required to maintain the desired orbit. Following the initial injection from the launch vehicle, similar, though usually larger, maneuvers are first needed to acquire the mission orbit. For low-earth orbiting satellites, this typically involves acquisition of the desired ground track and, for sun-synchronous orbits, adjustment of the local mean equatorial crossing time. Other considerations may warrant additional corrections, such as placement of the eccentricity vector for frozen orbits.

This analysis concentrates on developing analytical models for the in-plane maneuvers required to achieve and to maintain the orbit for a mission dedicated to mapping the particular region of the Earth. These along-track burns add or remove energy from the orbit, altering the semi-major axis and the eccentricity vector. By phasing the maneuvers during the acquisition phase, the actual ground track can be aligned with the desired path. In addition, to establish a frozen orbit, in which the eccentricity vector does not precess, the argument of perigee can be set to the required value (Chobotov & Karrenberg 1991). Subsequent periodic maneuvers throughout the maintenance phase must then compensate for the effects of atmospheric drag to ensure that the ground track remains within the desired tolerance.

Substantial research has been conducted regarding maneuvers in nearly circular orbits. The maneuver models developed in this paper are adapted from the work done by Cutting *et al.* (1978), for the SEASAT-A program, and the extensive analysis by Jones (1976) concerning optimal rendezvous solutions. The paper begins by discussing the drift of the ground track relative to the desired path resulting from off-nominal mean orbital parameters. A linearized model of that behavior is then developed. The subsequent section explores the relationship between atmospheric drag and the semi-major axis of the orbit. The remaining sections combine the analytical perturbation models with those for the maneuver parameters to provide a comprehensive strategy for ground-track acquisition and maintenance maneuver planning. Two spread sheet programs are developed for pre-flight planning and analysis. Then the simulations are executed for the ground track acquisition and maintenance maneuvers.

2. MODELING OF THE GROUND TRACK DRIFT

2.1 Ground track drift

The ground track refers to the path of the sub-satellite point, characterized at any time by latitude and longitude. As a satellite moves through its orbit, the Earth rotates eastward, and the ascending node precesses due to the J_2 perturbation. Beginning at an ascending node, after one complete revolution, the satellite passes over a different point on the Earth at the next ascending node, as illustrated in Figure 1.

This shift in the ground track from one pass to the next is determined by:

$$S = P_n(\omega_e - \dot{\Omega}) \tag{1}$$

where ω_e represents the rotation rate of the Earth; P_n represents the nodal period of the satellite:

$$P_n = 2\pi\sqrt{\frac{a^3}{\mu}}\left[1 - \frac{3}{2}J_2\left(\frac{R_e}{a}\right)^2(4\cos^2 i - 1)\right] \tag{2}$$

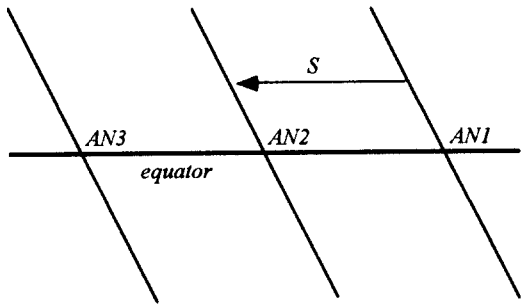

Figure 1. Shift of the Ground Track.

and $\dot{\Omega}$ represents the precession rate of the ascending node (Kalke 1994):

$$\dot{\Omega} = -\frac{3}{2} J_2 \sqrt{\frac{\mu}{a^3}} \left(\frac{R_e}{a} \right)^2 \frac{\cos i}{\left(1 - e^2\right)^2} \tag{3}$$

In these and all other equations, μ, J_2, and R_e represent the gravitational parameter, the second zonal harmonic coefficient, and the mean equatorial radius of the Earth. The orbit parameters a, e, and i represent the mean semi-major axis, eccentricity, and inclination. The value of S can be interpreted as the shift of the ground track per orbit revolution (rad/rev). The drift rate of the actual ground track relative to the ideal ground track can then be described by:

$$\delta S = S - S_{ideal} \tag{4}$$

From Equations (1) - (4), the drift rate is clearly a non-linear function of the actual and ideal orbital parameters. To align the actual ground track with the ideal path, the orbital elements must be adjusted in such a way as to produce the proper phasing of the drift. The next section outlines a method to relate drift rate changes directly to semi-major axis corrections.

2.2 Linearization

Solving Equation (4) for the actual mean orbital parameters required to yield the desired drift rate involves iteration, an unattractive feature for analytical models. Instead, take the Taylor series of S as defined by Equation (3), about an initial (though non-ideal) orbit, in two variables:

$$S(P_n, \dot{\Omega}) = S(P_{n_o}, \dot{\Omega}_o) + (P_n - P_{n_o}) \left. \frac{\partial S}{\partial P_n} \right|_{(P_{n_o}, \dot{\Omega}_o)} + (\dot{\Omega} - \dot{\Omega}_o) \left. \frac{\partial S}{\partial \dot{\Omega}} \right|_{(P_{n_o}, \dot{\Omega}_o)} \tag{5}$$

Substituting for the partial derivatives, subtracting S_{ideal} from both sides, and applying Equation (4) yields:

$$\delta S = \delta S_o + (\omega_e - \dot{\Omega}_o) \Delta P - P_{n_o} \Delta \dot{\Omega} \tag{6}$$

A change in the drift rate from that of the nominal orbit is then given by:

$$\Delta\delta S = \delta S - \delta S_o = A_1 \Delta P - A_2 \Delta\Omega \tag{7}$$

where the A_i notation has been introduced for compactness. Next, the equations for the nodal period and nodal precession rate must be linearized. Expressing the definitions in a modified form:

$$P_n(a) = \frac{2\pi}{\sqrt{\mu}} a^{\frac{3}{2}} - \frac{3\pi}{\sqrt{\mu}} J_2 R_e^2 (4\cos^2 i - 1) a^{-\frac{1}{2}} = B_1 a^{\frac{3}{2}} - B_2 a^{-\frac{1}{2}} \tag{8}$$

$$\dot{\Omega}(a) = -\frac{3}{2} \frac{J_2 R_e^2 \cos i \sqrt{\mu}}{\left(1 - e^2\right)^2} a^{-\frac{7}{2}} = B_3 a^{-\frac{7}{2}} \tag{9}$$

Again taking Taylor series, normalizing the resulting Δa by the initial semi-major axis a_o, and applying the binomial expansion theorem for small quantities yields:

$$\begin{aligned} \Delta P &= \frac{1}{2}\left\{ \left[3B_1 a_o^{\frac{3}{2}} + B_2 a_o^{-\frac{1}{2}}\right] \left(\frac{\Delta a}{a_o}\right) + \frac{3}{2}\left[B_1 a_o^{\frac{3}{2}} - B_2 a_o^{-\frac{1}{2}}\right] \left(\frac{\Delta a}{a_o}\right)^2 \right\} \\ &= \frac{1}{2}\left[C_1 R + C_2 R^2\right] \end{aligned} \tag{10}$$

$$\Delta\dot{\Omega} = -\frac{7}{2} B_3 a_o^{-\frac{7}{2}} \left[\left(\frac{\Delta a}{a_o}\right) - \frac{9}{2}\left(\frac{\Delta a}{a_o}\right)^2\right] = C_3 \left[R - \frac{9}{2} R^2\right] \tag{11}$$

Substituting these results into Equation (7) and combining terms produces a quadratic equation in R:

$$\left[\frac{1}{2} A_1 C_2 + \frac{9}{2} A_2 C_3\right] R^2 + \left[\frac{1}{2} A_1 C_1 - C_2 C_3\right] R - \Delta\delta S = D_1 R^2 + D_2 R - \Delta\delta S = 0 \tag{12}$$

which, given an initial orbit and $\Delta\delta S$, can be solved for R:

$$R = \frac{\Delta a}{a_o} = \frac{-D_2 \pm \sqrt{D_2^2 + 4 D_1 \Delta\delta S}}{2 D_1} \tag{13}$$

and thus, the Δa is required.

2.3 Effect of Atmospheric Drag

The motion of a satellite through the atmosphere creates a drag force acting opposite in direction to the velocity vector. This dissipative force removes energy from the orbit, causing the semi-major axis to decrease. The resulting mean decay rate depends on spacecraft characteristics and atmospheric density (Kalke 1994):

$$\dot{a} = -\frac{A}{m} C_d \rho \sqrt{\mu \cdot a} \tag{14}$$

where A is the spacecraft cross-sectional area normal to the velocity vector; m is the spacecraft mass; C_d is the drag coefficient; ρ is the mean density of the atmosphere at the current position; and a is the current mean semi-major axis.

Several models of varying degrees of complexity have been developed to estimate the density within the Earth's atmosphere as a function of altitude and time. This mission analysis employs the Marshall Spaceflight Center (MSFC)/J70 Orbital Atmospheric Density Model by Johnson & Smith (1985), which is a modified version of the Smithsonian Astrophysical Observatory's Jacchia 1970 model by Jacchia (1970), and has been developed by the National Aeronautics and Space Administration. Once the decay rate of the semi-major axis has been determined, the effect on the actual ground track relative to the ideal trace can be ascertained. From the initial value and the decay rate, the semi-major axis can be computed at any time t:

$$a(t) = a_o + \dot{a}(t - t_o) \tag{15}$$

Neglecting the change in mean inclination during the time period of interest, the new values for the nodal period and precession rate can be computed directly from the updated semi-major axis via Equations (2) and (3). Substituting the results into Equations (1) and (4) yields the revised relative drift rate at time t.

3. MANEUVER MODELING

Due to the near circularity of the orbits under consideration, Jones (1976) employs non-singular orbital elements. Those relevant to this analysis are:

$$\left\{ \frac{\Delta a}{a}, e_x, e_y \right\}$$

where

$$\begin{aligned} e_x &= e\cos\omega \\ e_y &= e\sin\omega \end{aligned} \tag{16}$$

and ω represents the argument of perigee.

The effects of radial and transverse ΔV_s on these orbital elements can be determined from the non-singular form of Lagrange's planetary equations:

$$\frac{\Delta a}{a} = \frac{2r}{h}\Delta V_t + \frac{2\mu a e}{h^2}\Delta e \tag{17}$$

$$\Delta e_x = \frac{p}{h}\sin(\omega + f)\Delta V_r + \left[2\frac{p}{h}\cos(\omega + f) + \frac{re}{h}\sin f \sin(\omega + f)\right]\Delta V_t \tag{18}$$

$$\Delta e_y = -\frac{p}{h}\cos(\omega + f)\Delta V_r + \left[2\frac{p}{h}\sin(\omega + f) - \frac{re}{h}\sin f \cos(\omega + f)\right]\Delta V_t \tag{19}$$

where the subscripts r and t refer to radial and transverse components, respectively; f represents the true anomaly; and r represents the geocentric radius. The semi-latus rectum and the angular momentum are defined as:

$$p = a(1 - e^2) \tag{20}$$

$$h = \sqrt{\mu p} \tag{21}$$

Furthermore, by linearizing these equations about a circular orbit ($e = 0$) of semi-major axis a_o, the equations reduce to:

$$\frac{\Delta a}{a_o} = 2\sqrt{\frac{a_o}{\mu}}\Delta V_t \tag{22}$$

$$\Delta e_x = \sin(\omega + f)\sqrt{\frac{a_o}{\mu}}\Delta V_r + 2\cos(\omega + f)\sqrt{\frac{a_o}{\mu}}\Delta V_t \tag{23}$$

$$\Delta e_y = -\cos(\omega + f)\sqrt{\frac{a_o}{\mu}}\Delta V_r + 2\sin(\omega + f)\sqrt{\frac{a_o}{\mu}}\Delta V_t \tag{24}$$

These equations now form the basis of the maneuver planning model. The solution algorithm is designed to provide the burn magnitude and location for each of the maneuvers, as well as the post-burn orbital elements.

To meet the objectives of the orbit acquisition phase, the drift rate of the ground track must be adjusted. After specifying the desired change in drift rate, the corresponding change in the semi-major axis is computed from Equation (13). The necessary ΔV can then be obtained from Equation (22):

$$\Delta V_t = \frac{1}{2}\frac{\Delta a}{a_o}\sqrt{\frac{\mu}{a_o}} \tag{25}$$

The desired adjustment requires a velocity increment only in the *transverse* direction (perpendicular to the radius vector in the direction of motion). The resulting change in the eccentricity vector can then be calculated using Equations (23) and (24). Observing that $\Delta V_r = 0$,

$$\Delta e_x = 2\cos(\omega + f)\sqrt{\frac{a_o}{\mu}}\Delta V_t \tag{26}$$

$$\Delta e_y = 2\sin(\omega + f)\sqrt{\frac{a_o}{\mu}}\Delta V_t \tag{27}$$

Each of these equations depends on the argument of latitude $(\omega + f)$ of the planned burn. The relative size of the change in each component of the eccentricity vector dictates the post-burn argument of perigee, ω_1:

$$\tan\omega_1 = \frac{e_{y_1}}{e_{x_1}} = \frac{e_{y_o} + \Delta e_y}{e_{x_o} + \Delta e_x} \tag{28}$$

Substituting Equations (26) and (27) into Equation (28), and applying trigonometric identities, the following expression can be derived:

$$\sin[(\omega_o + f_o) - \omega_1] = \frac{1}{2}\sqrt{\frac{\mu}{a_o}}\frac{\cos\omega_1}{\Delta V_t}(e_{x_o}\tan\omega_1 - e_{y_o}) \tag{29}$$

where the subscript o has been added to the components of the argument of latitude to indicate that those parameters refer to the pre-burn orbit. This equation can then be solved for the argument of

latitude of the burn,

$$(\omega_o + f_o) = \omega_1 + \sin^{-1}\left[\frac{1}{2}\sqrt{\frac{\mu}{a_o}}\frac{\cos\omega_1}{\Delta V_t}(e_{x_o}\tan\omega_1 - e_{y_o})\right] \tag{30}$$

The arcsine function, however, yields two solutions:

$$\sin^{-1} x = \alpha \Leftrightarrow \sin^{-1} x = 180^o - \alpha \tag{31}$$

Thus, for a single user-specified $\Delta\omega$, two solutions for the burn location yield the desired result, but produce two different post-burn eccentricities. The preferred argument of latitude for the burn must then be chosen in light of the effect on the orbital eccentricity.

From Equation (29), it also becomes evident that there must be a maximum value by which the argument of perigee can be changed in a single maneuver. Noting that the right-hand side of that equation must have an absolute value less than or equal to 1, and applying the definition of the eccentricity vector in Equation (16), along with appropriate trigonometric identities, the maximum change in ω can be determined from:

$$\sin\Delta\omega_{max} = \frac{2\Delta V_t}{e_o}\sqrt{\frac{a_o}{\mu}} \tag{32}$$

The fuel cost of an individual maneuver can be computed from the ΔV given in Equation (25) via the rocket equation:

$$\Delta m = m_{pre-burn}\left(1 - e^{-\Delta V_t/g\cdot I_{sp}}\right) \tag{33}$$

where g represents standard gravity at the Earth's surface, and I_{sp} represents the specific impulse of the on-board engines. Finally, the burn duration can be determined by:

$$\Delta t = \frac{\overline{m}\Delta V_t}{T} \tag{34}$$

where the bar over the m indicates that the average value of the spacecraft mass during the course of the burn should be used, and T represents the total thrust of the engines performing the maneuver.

4. GROUND TRACK ACQUISITION AND MAINTENANCE MANEUVER

4.1 Ground Track Acquisition Maneuver

In general, given an initial distance of the ground track from the desired trace, d_o, and calculating the drift rate, δS as outlined in the previous section, the relative position of the current ground track, d, can be determined at any point in time:

$$d(t) = d_o + (\delta S)R_e(t - t_o) \tag{35}$$

Table 1. Orbit and spacecraft parameters for the ground track acquisition maneuver.

	Initial	Ideal	Final
Ground Track Shift	-35.0	4.8	4.121
Semi-Major Axis(km)	7055.76	7063.27	7063.065
Eccentricity	0.0025	0.0010486	0.001582
Argument of Perigee(deg)	94.0	90.0	90.356
Spacecraft Mass(kg)	500	-	498.889
Total Impulsive Thrust(N)	16.7	-	16.7
Specific Impulse(sec)	180.0	-	180.0

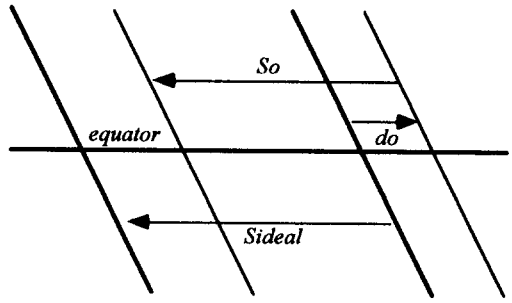

Figure 2. Ground Track Offset.

as shown in Figure 2.

The orbit acquisition phase seeks to reduce both the drift rate of the ground track and its distance from the ideal path to zero. To accomplish these goals, impulsive velocity increments in the radial and transverse directions are applied.

A ground track acquisition maneuver simulation is performed using spread sheet program that is developed using the modeling in previous section. Only in-track maneuvers are executed for changing semi-major axis, eccentricity, and argument of perigee. Table 1 shows the initial, ideal and final orbit parameters in the simulation. The ideal ground track shift, 4.8 km, in Table 1 is derived from the assumption that the ground track should be maintained within ± 5 km. The control bandwidth of the ground track is different for the spacecraft mission. Prasad *et al.* (1989) mentioned ± 14.8 km band for IRS program and Rosengren (1993) analyzed ± 1 km band for ERS-1 mission.

Five in-plane maneuvers are executed for achieving the final orbit parameters in Table 1. Each maneuver is executed in every 28-orbit revolution interval. Figure 3 shows the change of the semi-major axis during the orbit acquisition. There are small orbital decays in each 28-orbit revolution intervals. Figure 4 shows the change of the ground track shift during the orbit acquisition. The final ground track is 4.1 km east of the nominal ground track and this position is good for starting of routine ground track maintenance maneuver within ± 5 km band.

Figure 5 shows the change of eccentricity during ground track acquisition. The eccentricity is approached to the ideal frozen eccentricity throughout the maneuvers. Figure 6 shows the change of argument of perigee. The argument of perigee is decreased during each maneuver interval of 28-orbit

Table 2. Summary of the orbit acquisition maneuver.

Burn No.(rev.)	ΔSMA(km)	ΔV(m/s)	Δm(kg)	Burn Time(s)	$\omega + f$ (deg)
1(28)	1.544	0.823	0.233	24.6	229.788
2(28)	1.381	0.735	0.208	22.0	250.246
3(28)	2.918	1.553	0.439	46.4	257.454
4(28)	1.209	0.643	0.182	19.2	242.453
5(28)	0.322	0.171	0.048	5.1	203.560
Total 5(140)	7.374	3.926	1.111	117.3	-

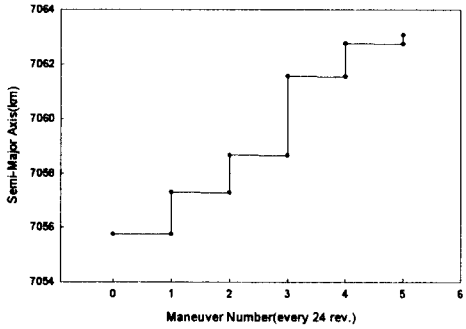

Figure 3. Change of semi-major axis.

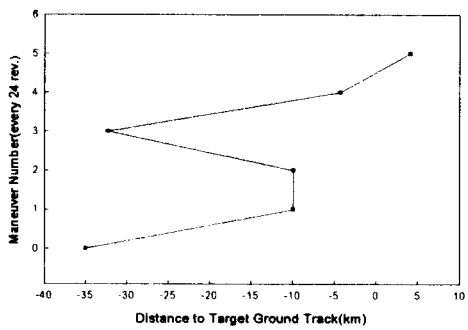

Figure 4. Change of ground track shift.

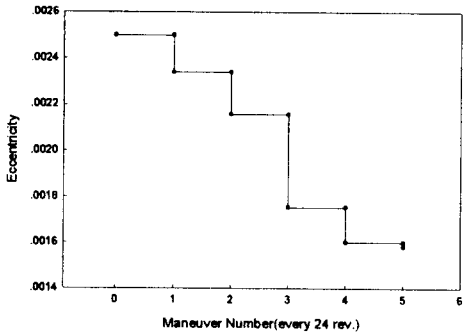

Figure 5. Change of eccentricity.

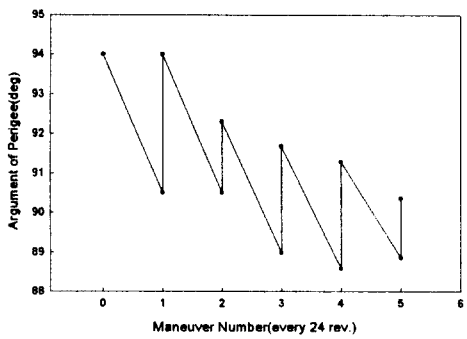

Figure 6. Change of argument of perigee.

revolution. The argument of perigee is also approached to the ideal frozen mean argument of perigee of 90°. The relation between frozen orbit eccentricity and argument of perigee, and the time variations of the frozen orbit parameters due to perturbations were analyzed by Lee & Lee (1997).

Table 2 shows the summary of the ground track acquisition maneuver. The argument of latitude, $\omega + f$, at the burn time is also shown in Table 2.

Table 3. Orbital elements and spacecraft parameters.

Parameters	Values
Mean Semi-Major Axis(km)	7063.270
Mean Eccentricity	0.0010486
Mean Inclination(deg)	98.127
Mean Argument of Perigee(deg)	90.000
Spacecraft Area(m^2)	8.250
Spacecraft Mass(kg)	400
Drag Coefficient	2.2
Total Propulsive Thrust(N)	16.7
Specific Impulse(sec)	180

4.2 Ground Track Maintenance Maneuver

As discussed previously, atmospheric drag monotonically removes energy from the orbit, causing the semi-major axis to decrease continuously. To meet the mission constraints, periodic maneuvers must be employed to counter this effect. Biasing the initial semi-major axis above the ideal value yields a longer interval between maneuvers, reducing the frequency of the necessary corrections.

To understand this behavior, consider first that the larger semi-major axis produces a longer orbital period. Neglecting the relatively small change in the nodal precession rate, the resulting effect on the ground track is given by Equation (1). The longer period, P_n, yields a larger shift in the ground track, which is measured positive westward. As a result, the ground track initially moves west relative to the ideal trace. By beginning the maneuver cycle with the actual ground track placed east of the intended path, and recognizing that atmospheric drag will cause the semi-major axis to decrease, the motion of the satellite begins to approach to the ideal orbit. Since drag continues to act, however, the semi-major axis will then fall below the ideal value, thus reversing the drift of the ground track. Then, the ground track moves to eastward. In that sense, maintaining the ground track of the LEO satellite within a certain bandwidth is very similar to maintaining the longitude of the GEO satellite within a certain station-keeping box.

Simulations for ground track maintenance maneuver are performed using spread sheet program that is developed using the modeling in previous section. The ground track bandwidth is set to ± 5 km in the simulations and the decay rate of the orbit is changed by setting the different initial air density. Table 3 shows the orbital elements and spacecraft parameters in the simulation.

Table 4 shows the summary of the ground track maintenance maneuver. Three different values of the air density are applied and the relating maneuver parameters are derived. The minimum and maximum air density values are adopted from Cappellari *et al.* (1976). The initial semi-major axis should be set to different value with respect to the decay rate of the orbit.

Figure 7 shows the profiles of the ground tracks for three different air drag values. The ground track initially evolves to westward from the eastern limit to the western limit, and then, evolves to eastward from the western limit to the eastern limit. Then, another ground track maintenance maneuver, i.e., orbit raising maneuver should be executed at eastern limit position. The ground track shift is directly related to the semi-major axis. Figure 8 shows the profiles of the semi-major axis for the three different cases. The maneuver cycle times are 13, 21, and 41 days each for the maximum, nominal, and minimum air drag. The more air density effects, the more ΔV is required for the ground

Table 4. Summary of ground track maintenance maneuver.

	Minimum	Nominal	Maximum
Air Density(Kg/m^3)	2.63E-14	1.00E-13	2.69E-13
Initial Semi-Major Axis(km)	7063.580	7063.476	7063.378
Initial Ground Track Shift(km)	4.8	4.8	4.8
Initial Decay Rate(m/day)	-5.5	-20.8	-56.0
Initial Drift Rate(kmE/rev)	-0.063	-0.121	-0.181
Final Semi-Major Axis(km)	7063.159	7063.060	7062.908
Maneuver Cycle(day)	13	21	41
Required Δa(km)	0.219	0.416	0.672
Required ΔV(m/sec)	0.116	0.221	0.357

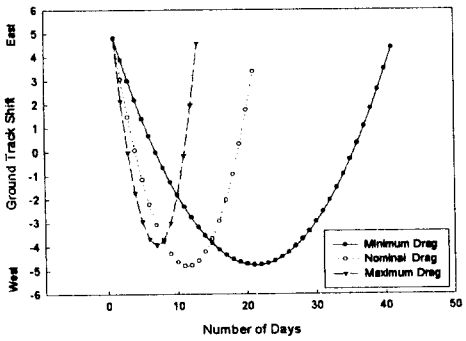

Figure 7. Profile of the Ground Track Shift.

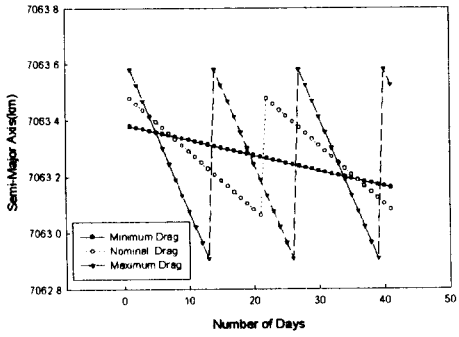

Figure 8. Profile of the Semi-major axis.

track maintenance.

When the actual ground track returns to the initial distance from the desired path, a maneuver is performed to reinitiate the cycle. This maneuver simply returns the drift rate to its initial value and direction by increasing the semi-major axis to the biased value. Thus, the velocity increment required can be found from Equations (13) and (23). As in the orbit acquisition case, only a transverse impulse is needed.

Since the mission orbit is frozen, however, the mean eccentricity and argument of perigee remain unaffected by perturbations. Consequently, the maintenance maneuver should be performed at a location such that the orientation of the eccentricity vector is unaffected. From Equation (30), it is clear that this can occur only if the burn takes place at perigee (f_o = 0°) or at apogee (f_o = 180°). The possible post-burn eccentricities can be determined using Equations (27) and (28), and the more appropriate apsis selected for the maneuver. The fuel use and duration can be calculated from Equations (34) and (35).

5. CONCLUSIONS

The strategy developed in this paper to determine the burn parameters for ground-track acquisition and maintenance has several advantages, including speed and simplicity. The use of the

linearized non-singular Lagrange equations allows analytical determination of the burn location without iteration. The implementation presented in the SEASAT-A analysis by Cutting *et al.* (1978) requires *a priori* knowledge of the eccentricity change. Since the primary goal of both the acquisition and maintenance phases involves the adjustment of the semi-major axis, the post-burn eccentricity becomes a consequential rather than a determinant factor. Thus, by returning to the basic model developed by Jones (1976), the correction burn location and ΔV can be derived from the parameters that the spacecraft mission analyst wishes to control, namely the drift rate of the ground track and the argument of perigee.

The primary limitation of the model also stems from the linearization of the non-singular Lagrange equations. The ΔV associated with the desired change in the semi-major axis exists in the transverse direction only. While reasonable, this assumption implies that the burn occurs while the spacecraft points in the nadir (anti-radial) direction, and that the along-track thrusters act along a line perpendicular to that direction. Non-zero pitch or yaw angles during actual burns will require slightly larger velocity increments than those calculated by this model.

Finally, the maneuvers planned by applying this strategy to the acquisition and maintenance of the mission orbit should serve as a baseline. Used as a pre-flight analysis and planning tool, this approach provides a comprehensive overview of the burn sequencing required to achieve the target orbit and the dynamics affecting the interval between maintenance maneuvers. Given the analytical nature of the models and the use of mean orbital elements, however, individual burns should ultimately be planned using higher fidelity numerical techniques. Higher fidelity numerical simulation will be performed later as a further study.

REFERENCES

Cappellari, J. O., Velez, C. E. & Fuchs, A. J. 1976, Mathematical Theory of the Goddard Trajectory Determination System, eds. J. O. Cappellari, C. E. Velez and A. J. Fuchs (GSFC: Maryland)

Chobotov, V. & Karrenberg, H. K. 1991, Orbital Mechanics, ed. V. Chobotov (AIAA: Washington), pp.291-296

Cutting, E., Born, G. H. & Frautnick, J. C. 1978, J. of the Astronautical Sciences, 26, 315

Jacchia, L. G. 1970, New Static Models of the Thermosphere and Exosphere with Empirical Temperature Profiles, Smithonian Astrophysical Observatory Special Report No.313

Jones, J. 1976, J. of the Astronautical Sciences, 24, 55

Johnson, D. & Smith, R. 1985, The MSFC/J70 Orbital Atmosphere Model and the Databases for the MSFC Solar Activity Prediction Technique, NASA-TM-86522

Kalke, J. 1994, Landsat 7 Mission Analysis Plan, Landsat 7 Program Information Release, U-S/C-L7-042

Lee, B.-S. & Lee, J.-S. 1997, J. of The Korean Society for Aeronautical and Space, 25, 126.

Prasad, P. R., Rao, S. V., Krishna, A., Padmanabhan, P. & Chandrasekhar, M. G. 1989, Acta Astronautica, 20, 103

Rosengren, M. 1993, Advances in the Astronautical Sciences, AAS 93-308, 84, 847

Wertz, J. R. 1991, Space Mission Analysis and Design, eds. J. R. Wertz, and W. J. Larson (Kluwer Academic Publishers: Dordrecht), pp.163-166